
Zn Vacancy-Regulated $\text{Zn}_{0.4}\text{Cd}_{0.6}\text{S}$ for Enhanced Charge Separation and Boosted Photocatalytic H_2O_2 Generation

Yuanyi Zhang, Yang Gu, Yuxin Lan, Zhenyu Wang, Wei Yan, Yingcong Wei and JingXu*

School of Physics and Electronic Engineering, Jiangsu University, Zhenjiang, Jiangsu, 212013, P. R. China

*Corresponding Author: JingXu. Email: xjing@ujs.edu.cn

1 Materials and Methods

1.1 Preparation of $\text{Zn}_V\text{-Zn}_{0.4}\text{Cd}_{0.6}\text{S-X}$ ($\text{Zn}_V\text{-ZCS-X}$)

During the experiment, 4 mmol of $\text{Zn}(\text{CH}_3\text{COO})_2 \cdot 2\text{H}_2\text{O}$ was dissolved in 30 mL of deionized water. Then, 6 mmol of $\text{Cd}(\text{CH}_3\text{COO})_2 \cdot 2\text{H}_2\text{O}$ and 10 mmol of L-cysteine were added successively, and the mixture was stirred for 30 minutes. Subsequently, the obtained mixture was transferred to a 50 mL reaction vessel and reacted at 180°C for 18 h. After the system cooled to room temperature, the reaction mixture was centrifuged at 9000 r/min for 5 min. To remove impurities, the product was rinsed several times, alternately washed with deionized water and absolute ethanol. The collected precipitate was subsequently dried in a vacuum oven at 60°C for 12 h to obtain the $\text{Zn}_V\text{-Zn}_{0.4}\text{Cd}_{0.6}\text{S-10}$ sample, denoted as $\text{Zn}_V\text{-ZCS-10}$. Under identical conditions, a series of $\text{Zn}_V\text{-ZCS-X}$ samples were prepared by adjusting the amount of L-cysteine added, where $X = 6.5, 8, 10$, and 13.5 .

1.2 Chemicals and Reagents

Cadmium acetate dihydrate ($\text{Cd}(\text{CH}_3\text{COO})_2 \cdot 2\text{H}_2\text{O}$, $\geq 99.9\%$), zinc acetate dihydrate ($\text{Zn}(\text{CH}_3\text{COO})_2 \cdot 2\text{H}_2\text{O}$, $\geq 99.0\%$) and L-cysteine ($\text{C}_3\text{H}_7\text{NO}_2\text{S}$, $\geq 99\%$) were purchased from Shanghai Macklin Biochemical Co., Ltd., Shanghai, China. Thioacetamide (TAA, $\text{C}_2\text{H}_5\text{NS}$, $\geq 99.0\%$) was obtained from Shanghai Reagent Co., Ltd., China. All experiments were conducted using ultrapure water. All the aforementioned chemicals were utilized as received, without any further purification.

1.3 Preparation of $\text{Zn}_{0.4}\text{Cd}_{0.6}\text{S}$ (ZCS)

To experiment, 4 mmol of $\text{Zn}(\text{CH}_3\text{COO})_2 \cdot 2\text{H}_2\text{O}$ should be dissolved in a solution consisting of $\text{C}_2\text{H}_8\text{N}_2$ and deionized water (25 mL water and 25 mL $\text{C}_2\text{H}_8\text{N}_2$), followed by the addition of 6 mmol of $\text{Cd}(\text{CH}_3\text{COO})_2 \cdot 2\text{H}_2\text{O}$. Upon clarification of the solution, 13 mmol TAA should be introduced, with stirring for 30 minutes. Subsequently, the resulting mixture is to be transferred into a 50 mL reactor and subjected to a reaction at a temperature of 220°C for 24 hours. Following cooling of the reactor to room temperature, it must undergo centrifugation at a rate of 9000 r/min for 5 minutes before undergoing multiple washes with deionized water and anhydrous ethanol. The resultant sediment is then to be placed within a vacuum drying box set at a temperature of 60°C for an overall duration totaling up to 12 hours to yield the final sample comprising the $\text{Zn}_{0.4}\text{Cd}_{0.6}\text{S}$ solid solution.

1.4 Photocatalytic production of H_2O_2

The specific steps for photocatalytic H_2O_2 production are as follows: A total of 10 mg of catalyst was dispersed in a 100 mL three-neck flat-bottom flask equipped with 19/26 ground-glass joints, containing 45 mL of deionized water and 5 mL of lactic acid (LA). After sealing, the suspension was ultrasonicated and

magnetically stirred to ensure uniform dispersion of the catalyst. Subsequently, O₂ was continuously bubbled through the suspension for 15 min before irradiation. The reaction mixture was then irradiated from the front using a 425 nm LED light source, and the measured irradiance at the sample position was 44 mW/cm². The photocatalytic reaction was carried out for 1 h. Aliquots of 1 mL were collected every 20 minutes and passed through a 0.22 µm filter membrane to remove the catalyst particles.

The H₂O₂ concentration was quantified by the iodometric method: Take 50 µL of the above filtered supernatant and mix it with 0.5 mL of 0.4 M potassium iodide and 0.5 mL of 0.1 M potassium hydrogen phthalate. Allow the mixture to react thoroughly by placing it in the dark for 30 minutes. Under acidic conditions ($\text{H}_2\text{O}_2 + 2\text{I}^- + 2\text{H}^+ \rightarrow \text{I}_2 + 2\text{H}_2\text{O}$), the generated I₂ exhibits a characteristic absorption peak at approximately 350 nm. The absorbance is measured using UV-Vis absorption spectroscopy, and the H₂O₂ content produced at each stage is calculated using the calibration curve for H₂O₂ quantification (Figure. S5).

Cycling experiment procedure: After each reaction, the catalyst was collected by centrifugation, thoroughly washed with deionized water and anhydrous ethanol, and then used for the next cycling experiment. Due to catalyst loss after the third cycle, we replenished the catalyst to a total mass of 10 mg before the fourth cycle experiment.

2 Characterization

X-ray diffraction (XRD) patterns were recorded on a Bruker D2 Phaser diffractometer using Cu Kα radiation ($\lambda = 1.5418 \text{ \AA}$) at 40 kV and 40 mA. Data were collected in the 2θ range of 10–80° with a step size of 0.02° and a scan speed of 2°/min.

Scanning electron microscopy (SEM) images were obtained on a JEOL JSM-7001F field-emission SEM at an accelerating voltage of 15 kV; secondary-electron (SE) images were mainly used and backscattered-electron (BSE) images were taken when compositional contrast was needed. Transmission electron microscopy (TEM) images and energy-dispersive X-ray spectroscopy (EDS) elemental maps were acquired on a JEOL JEM-2100 transmission electron microscope operated at 200 kV. Mapping was performed with a probe current of ~0.8 nA and a dwell time of ~5 µs per pixel. X-ray photoelectron spectroscopy (XPS) was performed on a Thermo Scientific K-Alpha instrument with Al Kα radiation ($h\nu = 1486.6 \text{ eV}$). Survey spectra were recorded with a pass energy of 150 eV and high-resolution spectra with a pass energy of 20 eV. All binding energies were calibrated by referencing the C 1s peak to 284.80 eV. XPS data were processed using Avantage with a Shirley background and Gaussian-Lorentzian peak shapes for fitting. Diffuse reflectance UV-Vis spectra (DRS) were measured on a Shimadzu UV-2550 spectrometer equipped with an integrating sphere; BaSO₄ was used as the reference. The reflectance data were converted to the Kubelka-Munk function for band-gap estimation. Photoluminescence (PL) spectra were collected on a JASCO FP-6500 fluorescence spectrophotometer using an excitation wavelength of 525 nm and slit widths of 5 nm for both excitation and emission. Photoelectrochemical measurements were carried out on a CHI660B potentiostat in a conventional three-electrode configuration with a Pt plate counter electrode and an Ag/AgCl (saturated KCl) reference electrode. Working electrodes were prepared by drop-casting a catalyst suspension (5 mg catalyst in 1 mL ethanol) onto fluorine-doped tin oxide (FTO) glass (active area = 1.76 cm²) and drying at 60 °C; the resulting catalyst loading was approximately 2.84 mg/cm². Transient photocurrent responses were recorded under chopped AM1.5G-simulated illumination (300 W Xe lamp with AM1.5G filter, 100 mW/cm²) using 10 s on / 10 s off cycles at 0 V vs. Ag/AgCl. Electrochemical impedance spectroscopy (EIS) measurements were performed at open-circuit potential with an AC

amplitude of 10 mV over the frequency range 100 kHz–0.1 Hz in 0.1 M Na₂SO₄. Mott-Schottky measurements were carried out in a conventional three-electrode configuration using the same electrolyte environment as that used for EIS. The catalyst-coated FTO electrode was used as the working electrode, with a Pt plate as the counter electrode and Ag/AgCl (saturated KCl) as the reference electrode. The electrolyte was 0.1 M Na₂SO₄ aqueous solution at pH 7. The measurements were performed at frequencies of 400, 600, and 800 Hz.

3 Apparent Quantum Yield (AQY) Measurement

Photocatalytic H₂O₂ activity was evaluated using 30 W LED light sources with different wavelengths (365, 405, 425, 520, and 920 nm). Under identical photocatalytic conditions, the AQY was calculated according to the following equation:

$$AQY(\%) = \frac{2 \times v \times N_A \times h \times c}{I \times A \times \lambda} \times 100\% \quad (1)$$

where v is the generation rate of H₂O₂ (mol/s), which was obtained from the slope of the initial linear region of the H₂O₂ evolution curve (Figure S5), N_A is Avogadro's constant, h is Planck's constant, c is the speed of light, I is the incident light power density (W/m²), A is the irradiation area (m²), and λ is the incident wavelength, converted into meters for calculation..

The irradiance spectrum of the 365, 405, 425, 520, 920 nm LED used in this work is provided in Figure S4. The 425 nm LED light emission spans from 395 to 465 nm, and the measured irradiance at the sample position is 44 mW/cm². Based on the measured photon flux. For the 425 nm LED, the incident photon flux was obtained from the measured spectral irradiance over the emission window rather than from a single nominal wavelength value.

4 ICP-OES Measurement

To further provide quantitative compositional evidence for Zn-vacancy formation, ICP-OES measurements were performed for pristine ZCS and Zn_V-ZCS-10. As summarized in Table S1, the Zn mass fraction of Zn_V-ZCS-10 is 16.7802 wt%, which is lower than that of pristine ZCS, 20.9028 wt%. The relative Zn deficiency was calculated according to the following equation:

$$\text{Relative Zn deficiency} = W_{Zn,ZCS} - W_{Zn,Zn_V-ZCS-10} \quad (2)$$

The relative Zn deficiency in Zn_V-ZCS-10 is therefore estimated to be approximately 4.1226 wt% compared with pristine ZCS. This result provides quantitative compositional evidence for the formation of Zn vacancies.

Table S1: ICP-OES results of ZCS and Zn_V-ZCS-X.

Sample	Test element	ICP reading	Zn content (wt%)	Relative Zn deficiency (wt%)
ZCS	Zn	3.9130 mg/L	20.9028	---
Zn _V -ZCS-13.5	Zn	7.8000 mg/L	16.6382	4.2646
Zn_V-ZCS-10	Zn	7.3430 mg/L	16.7802	4.1226
Zn _V -ZCS-8	Zn	7.4590 mg/L	17.7934	3.1094
Zn _V -ZCS-6.5	Zn	8.9740 mg/L	18.9165	1.9863

5 The Determination of the Band Structures

The flat-band potential was determined from the x-intercept of the Mott–Schottky plot [1]. Potentials measured versus Ag/AgCl were converted to the NHE scale using

$$E_{CB,NHE} = E_{Ag/AgCl} + 0.197 \quad (3)$$

at 25 °C [2]. For the n-type semiconductor, the conduction-band position was estimated from the flat-band potential, and the valence-band position was calculated from

$$E_{VB} = E_{CB} + E_g \quad (4)$$

where E_g was obtained from the UV-vis results [3]. The calculated values are therefore presented as estimated band alignment [3].

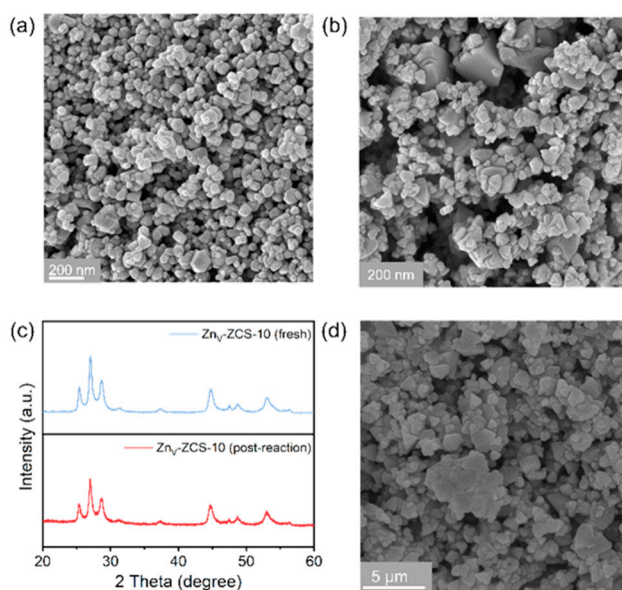


Figure S1: (a) SEM image of ZCS; (b) SEM image of fresh Zn_V-ZCS-10; (c) XRD patterns of fresh and post-reaction Zn_V-ZCS-10 samples; (d) SEM image of post-reaction Zn_V-ZCS-10.

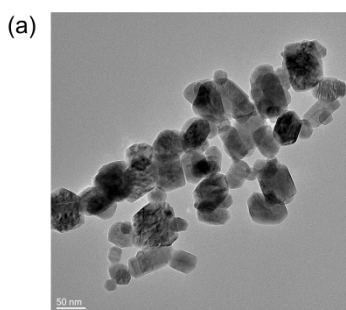


Figure S2: TEM image of ZCS.

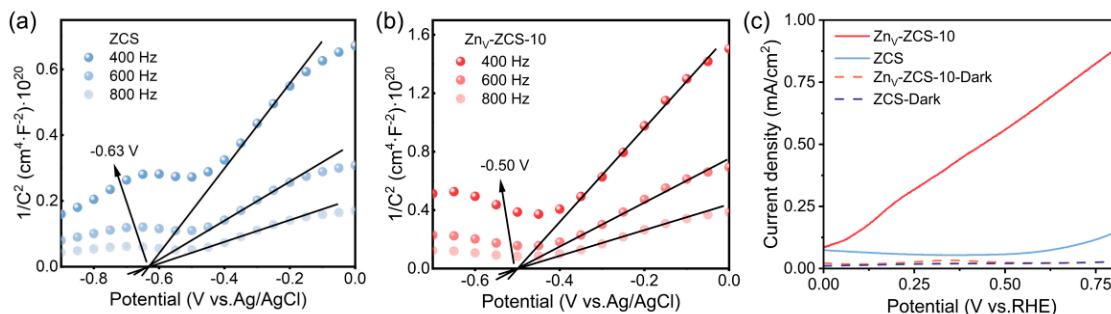


Figure S3: (a) Mott-Schottky plots of ZCS at different frequencies (400, 600, 800 Hz); (b) Mott-Schottky plots of ZnV-ZCS-10 at different frequencies (400, 600, 800 Hz); (c) Linear sweep voltammetry (LSV) of ZCS and ZnV-ZCS-10 samples.

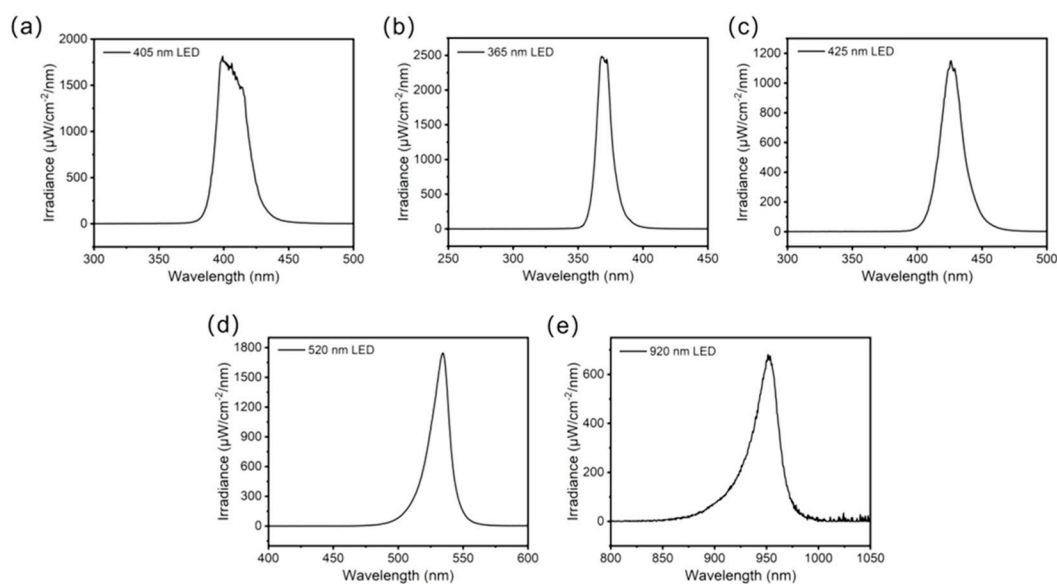


Figure S4: The irradiance spectrum of 30 W 365, 405, 425, 520, 920 nm LED light source.

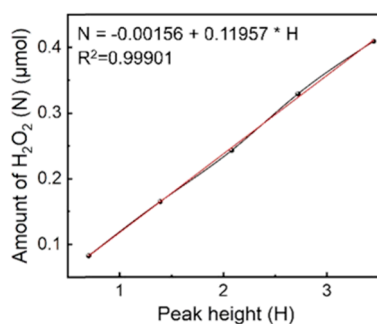


Figure S5: Standard curve of DRS absorption peak versus H₂O₂ content.

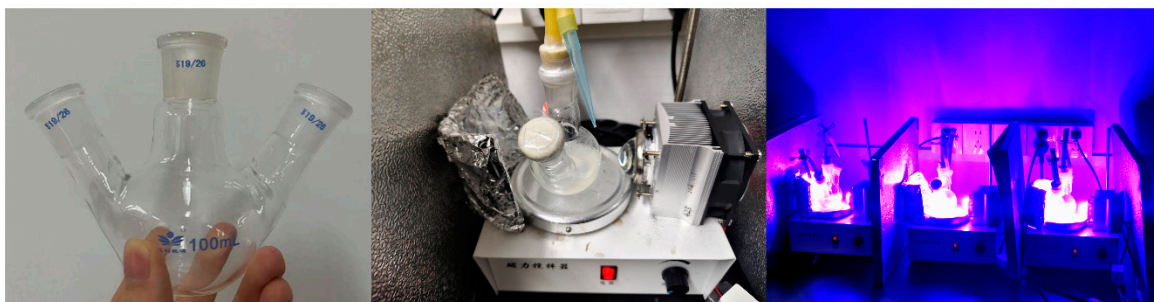


Figure S6: Photograph of the reactor used for photocatalytic H₂O₂ production.

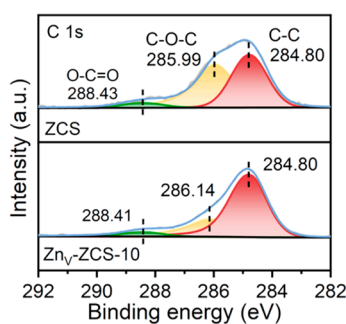


Figure S7: High-resolution C 1s spectra of ZCS and Zn_V-ZCS-10.

Table S2: Comparison of H₂O₂ production performance of sulfide-based photocatalysts.

Representative study	Photocatalyst / defect engineering	H ₂ O ₂ productivity (mmol/g/h)	Sacrificial agent
[4]	S vacancies in ZnIn ₂ S ₄ -based heterojunction	3.20	No
[5]	Surface In vacancies in In ₂ S ₃	4.77 ± 0.05	Trimethylamine (TEA)
[6]	S vacancies in ZnCdS@PDA hollow nanocages	45.5	----
[7]	Ag-modified sulfur-vacancy-rich ultrathin ZnIn ₂ S ₄ nanosheets	8.982	Isopropanol (IPA)
[8]	Ni-doped ZnS hollow nanocubes with sulfur vacancies	5.649	----
[9]	CaIn ₂ S ₄ with sulfur vacancies	0.7362	Ethanol
[10]	CdS nanorods with congenital and acquired sulfur vacancies	2.975	isopropanol (IPA)
[11]	CdS nanorods with sulfur vacancies under piezo-photocatalytic coupling	1.631	----
[12]	Defective ZrS ₃ nanobelts with disulfide/sulfide vacancies	1.56 ± 0.03	Benzylamine and benzyl alcohol
This work	Zn _V -ZCS-10	44.39	lactic acid

Table S3: Atomic ratios of each element of ZCS and Zn_v-ZCS-10.

Atomic ratios of each element of ZCS				
Name	BE (eV)	FWHM (eV)	Area (CPS-eV)	Atomic %
C 1s	284.80	1.44	32478.56	12.40
C 1s Scan A	288.43	1.64	3805.71	1.46
C 1s Scan B	285.99	1.58	34675.72	13.25
Cd 3d	404.50	0.96	823795.75	11.75
Cd 3d Scan A	411.25	0.95	558095.67	8.00
Zn 2p	1021.53	1.28	543389.65	13.08
Zn 2p Scan A	1044.52	1.36	184546.96	4.60
S 2p	160.98	0.95	130720.85	24.59
S 2p Scan A	162.19	0.94	57809.12	10.88
Atomic ratios of each element of Zn _v -ZCS-10				
Name	BE (eV)	FWHM (eV)	Area (CPS-eV)	Atomic %
C 1s	284.80	1.51	72302.73	27.41
C 1s Scan A	286.14	1.84	31461.09	11.94
C 1s Scan B	288.41	1.61	6398.16	2.43
Cd 3d	404.83	0.95	719755.98	10.20
Cd 3d Scan A	411.58	0.95	489748.67	6.97
Zn 2p	1021.73	1.24	347571.70	8.31
Zn 2p Scan A	1044.71	1.35	117570.34	2.91
S2p	161.27	0.93	99790.61	18.65
S 2p Scan A	162.50	0.87	59801.15	11.18

8 Characterization of the Sample after the Reaction

To further examine the structural stability of Zn_v-ZCS-10 after the photocatalytic reaction, XRD and SEM analyses were performed on the post-reaction catalyst. As shown in Figure S1c, the main diffraction features of Zn_v-ZCS-10 are retained in the post-reaction sample compared with the fresh sample, suggesting that no obvious phase transformation occurred during the cyclic photocatalytic test. In addition, the SEM image of the post-reaction Zn_v-ZCS-10 sample shows that the particulate morphology is largely maintained compared with the fresh Zn_v-ZCS-10 sample (Figure S1d). These results further support the phase and morphology stability of Zn_v-ZCS-10 under the present reaction conditions

Reference

1. Cardon F, Gomes W. On the determination of the flat-band potential of a semiconductor in contact with a metal or an electrolyte from the Mott-Schottky plot. *J Phys D Appl Phys.* 1978;11(4):L63–67.
2. Shao Q, Lin H, Shao M. Determining Locations of Conduction Bands and Valence Bands of Semiconductor Nanoparticles Based on Their Band Gaps. *ACS Omega.* 2020;5(18):10297–300. <https://doi.org/10.1021/acsomega.9b04238>
3. Hankin A, Bedoya-Lora F, Alexander J, Regoutz A, Kelsall G. Flat band potential determination: avoiding the pitfalls. *J Mater Chem A.* 2019;7(45):26162–26176. <https://doi.org/10.1039/c9ta09569a>
4. Gao Z, Liu F, Chen Z, Song Q, Cullen PJ, Zhang X, et al. Defect-modulated oxygen adsorption and Z-scheme charge transfer for highly selective H₂O₂ photosynthesis in pure water. *Nat Commun.* 2025;16(1):8889. <https://doi.org/10.1038/s41467-025-64166-8>

-
5. Zhu Q, Su J, Lin G, Li G, Zhuo Z, Wang W, et al. Surface indium vacancies promote photocatalytic H₂O₂ production over In₂S₃. *Nat Commun.* 2025;16(1):10501. <https://doi.org/10.1038/s41467-025-65538-w>
 6. Feng C, Zhang L. Microdroplet assisted hollow ZnCdS@PDA nanocages' synergistic confinement effect for promoting photocatalytic H₂O₂ production. *Mater Horiz.* 2024;11(6):1515–1527. <https://doi.org/10.1039/d3mh01915b>
 7. He Z, Li L, Pang Y, Cui M, Lin Y, Xie T. Ag-modified sulfur vacancy-rich ZnIn₂S₄ ultrathin Nanosheets promote oxygen activation for efficient photocatalytic hydrogen peroxide synthesis. *J Colloid Interface Sci.* 2025;700:138353. <https://doi.org/10.1016/j.jcis.2025.138353>
 8. Xi Y, Zhang C, Tu W, Guo Y, Bao T, Zou Y, et al. Modulating Active Hydrogen Supply and O₂ Adsorption: Sulfur Vacancy Matters for Boosting H₂O₂ Photosynthesis Performance. *Angew Chem Int Ed Engl.* 2025;64(25):e202505046. <https://doi.org/10.1002/anie.202505046>
 9. Mao Y, Zhang J, Zhao Y, Wei X, Jiang D, Zhu L, et al. An efficient improvement for photocatalytic hydrogen peroxide production: Sulfur vacancies in CaIn₂S₄. *J Colloid Interface Sci.* 2025;694:137614. <https://doi.org/10.1016/j.jcis.2025.137614>
 10. Zhang Y, Huang H, Wang L, Zhang X, Zhu Z, Wang J, et al. Cooperation of congenital and acquisitus sulfur vacancy for excellent photocatalytic hydrogen peroxide evolution of CdS nanorods from air. *Chem Eng J.* 2023;454:140420. <https://doi.org/10.1016/j.cej.2022.140420>
 11. Zhang Y, Wang L, Huang H, Hu C, Zhang X, Wang C, et al. Water flow induced piezoelectric polarization and sulfur vacancy boosting photocatalytic hydrogen peroxide evolution of cadmium sulfide nanorods. *Appl Catal B Environ Energy.* 2023;331:122714. <https://doi.org/10.1016/j.apcatb.2023.122714>
 12. Tian Z, Han C, Zhao Y, Dai W, Lian X, Wang Y, et al. Efficient photocatalytic hydrogen peroxide generation coupled with selective benzylamine oxidation over defective ZrS₃ nanobelts. *Nat Commun.* 2021;12(1):2039. <https://doi.org/10.1038/s41467-021-22394-8>